ISTITUTO NAZIONALE DI RICERCA METROLOGICA
Repository Istituzionale

Corrections of the travelling-fringe period for the interference of aberrated beams

(Article begins on next page)

26 November 2024

Corrections of the travelling-fringe period for the interference of aberrated beams

G Mana and C P Sasso

INRIM – Istituto Nazionale di Ricerca Metrologica, Str. delle cacce 91, 10135 Torino, Italy

E-mail: `g.mana@inrim.it`

Abstract.   When laser beams are used for length measurements by interferometry and the realisation of the meter, they are approximated by plane waves. Hence, from the measured frequency, the dispersion relation of plane waves gives the wavelength in a vacuum and, consequently, the period of the interference signal. However, this relation does not hold exactly and the wavelength is not a well-defined quantity. Aberrations of the wavefront and intensity profiles bias the phase accumulation and originate measurement errors. This paper gives the corrections for the period of the integrated interference of aberrated paraxial beams.

2

1. Introduction

A practical realisation of the metre is the wavefront spacing λ of laser beams whose frequency ν is linked to primary frequency standards [1]. For the primary measurements, two-beam interferometers are used, where the reference arm is fixed and the measurement one is continuously changed while sensing the interference fringes, whose period is assumed to be equal to λ. The dispersion relation for monochromatic plane waves in vacuum $\lambda = c/\nu$ – where the speed of light $c = 299792458$ ms^{-1} is prescribed by the International System of units – relates wavelength and frequency. However, plane waves are never realised in practice and limited monochromaticity [2–5], geometric phase [6–8], and diffraction [9–22] threaten the $\lambda = c/\nu$ relationship.

In addition to length metrology, the kilogram realization [23], gravimetry [13, 15, 17], precision γ-ray spectroscopy [24], the measurements of the Si lattice parameter [22, 25] and molar volume [18, 19, 26], and the foreseen space-based gravitational wave detector LISA [27, 28] need low-noise, sensitive, and accurate measurements and require more reliable determinations of the accumulated phase and fringe period. Some of these applications need only stable and low-noise signals. In this case, our work helps to quantify the phase noise induced by the coupling of the alignment jitter to the wavefront aberrations [29].

Aberrations are this paper's focus. Because of them, the wavefronts bend, their spacing varies from one point to another, and the wavelength is badly defined. Therefore, optical interferometry must rely on an effective wavelength, λ_e, that depends on how measurements are carried out.

We consider two-beam interferometers where the interference pattern is integrated over an infinite detection plane. In the case of misaligned Gaussian beams it is possible to calculate the interference phase for arbitrary and mismatched parameters [30]. Furthermore, if the beams are paraxial, but matched, the fractional correction of the fringe period – which, typically, ranges from parts in 10^{-7} to parts in 10^{-9} – is proportional to the trace of the second central-moment of the angular power spectrum of the interfering beams [31,32].

A combined X-ray and optical interferometer showed wavefront errors and local wavelength variations as large as ± 20 nm [33] and $\pm 10^{-8}\lambda$ [34]. Surpris-ingly, a numerical analysis brought into light that, on the average, the increased spread of the angular spectra does not affect the period of the travelling fringes [35].

Since these findings could not be explained physically, we carried out an analytical analysis of the interference of two (slightly) aberrated Gaussian beams with the purpose to exclude that it is specific to the numerical examples considered and to unveil its origin.

In section 2 we establish the modal spectrum representation, using the Hermite-Gauss modes as a basis [36, 37]. Section 3 uses this decomposition to study the interference of aberrated beams and to calculate the period of their interference. Section 4 investigates the interference of matched and mismatched Gaussian beams. Eventually, in section 5, we average the correction for the fringe period over white modal spectra constrained to fixed root-mean-square aberrations. The results confirm that the average correction does not depend on the aberrations.

2. Hermite-Gauss modes

The Hermite-Gauss beams, or TEM$_{lm}$ mode having rectangular symmetry,

$$u_{lm}(\xi_1, \xi_2; \zeta) = u_l(\xi_1; \zeta)u_m(\xi_2; \zeta), \qquad (1a)$$

form a complete orthogonal base for the separable solutions of the paraxial approximation of the scalar wave equation [37]. In $(1a)$ [38]

$$u_n(\xi; \zeta) = \frac{c_n}{\sqrt[4]{1 + \zeta^2}} \mathrm{H}_n\left(\frac{\sqrt{2}\xi}{\sqrt{1 + \zeta^2}}\right) \times$$
$$\times \exp\left[-\frac{\xi^2(1 + \mathrm{i}\zeta)}{1 + \zeta^2} + \frac{\mathrm{i}(2n + 1)}{2}\arctan(\zeta)\right], \quad (1b)$$

where

$$c_n = \sqrt{\frac{\sqrt{2/\pi}}{2^n n!}} \qquad (1c)$$

is the normalising factor and $\mathrm{H}_n(\xi)$ is the Hermite polynomial of degree n. Also, we omitted the plane wave $\mathrm{e}^{-\mathrm{i}kz + \mathrm{i}\omega t}$ term – where $k = \omega/c$ is the wave-number, ω is the angular frequency, z is the propagation distance, and t is time – and used the dimensionless coordinates $\xi_{1,2} = x_{1,2}/w_0$ and $\zeta = z/z_R$, where $x_{1,2}$ are the transverse coordinates, w_0 is the radius of the u_0's waist (which occurs at $\zeta = 0$), and $z_R = kw_0^2/2$ is the Rayleigh distance. In the following, we restrict the study to a single

transverse dimension. The extension to two orthogonal dimensions is straightforward.

Orthogonality and completeness mean that any separable paraxial beam can be written as a superposition of TEM_l modes as

$$\psi(\xi;\zeta) \propto u_0(\xi;\zeta) + \sum_{n \geq 1} a_n u_n(\xi;\zeta), \tag{2}$$

where, without loss of generality, the (possibly complex) coefficients,

$$a_n = \frac{\displaystyle\int_{-\infty}^{+\infty} \psi(\xi;0)u_n(\xi;0)}{\displaystyle\int_{-\infty}^{+\infty} \psi(\xi;0)u_0(\xi;0)\,\mathrm{d}\xi}, \tag{3}$$

are evaluated in $\zeta = 0$.

Since the w_0 value and the z-axis direction and origin are arbitrary, the representation (2) is not unique. For instance, we can set $w_0 = 2/(k\theta_0)$, where θ_0^2 is the second central moment of the ψ's angular spectrum, $\zeta = 0$ at the ψ's waist, and the z axis collinear to the ψ's axis. This means that the representation's TEM_0 mode is the best Gaussian beam fitting ψ.

2.1. Mismatched Gaussian beams

With these choices, the representation of a Gaussian beam is $a_n = \delta_{n0}$, where δ_{nm} is the Kronecker delta function. Different choices of the u_n's axis and waist location are possible. In this case, mismatches occur because of lateral displacements, tilts, and different waist location. Provided the mismatches are small, only a few low-order modes need to be considered.

2.1.1. Wavefront tilt. By application of (3), the beam,

$$\psi(\xi;0) = \exp\left(-\xi^2 - \mathrm{i}\tilde{\alpha}\xi\right), \tag{4a}$$

tilted at the $\alpha = \tilde{\alpha}/(kw_0)$ angle, where $\tilde{\alpha}^2 \ll 1$, can be expanded as

$$\psi(\xi;\zeta) \propto u_0(\xi;\zeta) - \frac{\mathrm{i}\tilde{\alpha}}{2}u_1(\xi;\zeta) - \frac{\tilde{\alpha}^2}{4\sqrt{2}}u_2(\xi;\zeta) + ... \tag{4b}$$

By observing that, in the series expansion of $\exp(-\mathrm{i}\tilde{\alpha}\xi)$, the $\tilde{\alpha}$ powers higher than two multiply ξ^3 and higher powers, the coefficients of the u_n modes higher than u_2 are proportional to $\tilde{\alpha}^3$ and higher powers. Similar considerations hold in the following.

2.1.2. Beam axis mismatch. The beam,

$$\psi(\xi;0) = \exp\left[-(\xi - \xi_0)^2\right], \tag{5a}$$

laterally displaced by a small amount ξ_0, can be expanded as

$$\psi(\xi;\zeta) \propto u_0(\xi;\zeta) + \xi_0 u_1(\xi;\zeta) + \frac{\xi_0^2}{\sqrt{2}}u_2(\xi;\zeta) + ... \tag{5b}$$

2.1.3. Waist location mismatch. The beam

$$\psi(\xi;0) = \exp\left[-\xi^2/(1 - \mathrm{i}\zeta_0^2)\right], \tag{6a}$$

whose waist is located at $\zeta = -\zeta_0$, where $\zeta_0^2 \ll 1$, can be expanded as

$$\psi(\xi;\zeta) \propto u_0(\xi;\zeta) - \frac{\zeta_0(2\mathrm{i} - \zeta_0)}{4\sqrt{2}}u_2(\xi;\zeta)$$
$$- \sqrt{\frac{3}{2}}\frac{\zeta_0^2}{8}u_4(\xi;\zeta) + ... \tag{6b}$$

2.1.4. Waist radius mismatch. The beam

$$\psi(\xi;0) = \exp\left[-\xi^2/(1 + \upsilon)^2\right], \tag{7a}$$

whose waist radius is $(1 + \upsilon)w_0$, where $\upsilon^2 \ll 1$, can be expanded as

$$\psi(\xi;\zeta) \propto u_0(\xi;\zeta) + \frac{\upsilon(2 - \upsilon)}{2\sqrt{2}}u_2(\xi;\zeta)$$
$$+ \sqrt{\frac{3}{2}}\frac{\upsilon^2}{2}u_4(\xi;\zeta) + ... \tag{7b}$$

2.1.5. Wavefront curvature mismatch. The beam

$$\psi(\xi;0) = \exp\left(-\xi^2 - \mathrm{i}\kappa\xi^2\right) \tag{8a}$$

where $\kappa^2 \ll 1$, can be expanded as

$$\psi(\xi;\zeta) \propto u_0(\xi;\zeta) - \frac{\kappa(2\mathrm{i} + \kappa)}{4\sqrt{2}}u_2(\xi;\zeta)$$
$$- \sqrt{\frac{3}{2}}\frac{\kappa^2}{8}u_4(\xi;\zeta) + ... \tag{8b}$$

It is worth noting that κ is the wavefront curvature at $\zeta = 0$. The beam waist is located at $\zeta = -\kappa$ or $\zeta = -(1 - \kappa^2)/\kappa$ and has radius $(1 - \kappa^2/2)w_0$ or κw_0, respectively.

3. Correction for the interference period

A two-beam interferometer displaces axially a measure beam ψ_{ms} (the one travelling through the variable arm) against a ψ_{rf} reference (the one travelling through the fixed arm) by s. By leaving out the $\exp(-\mathrm{i}kz_D)$ and $\exp[-\mathrm{i}k(z_D + s)]$ terms, where $z = z_D$ is the observation plane, the interference signal, integrated over an infinite-area detector, is

$$I(\varsigma) = \int_{-\infty}^{+\infty} |\psi_{\text{ms}}(\xi;\zeta_D) + \psi_{\text{rf}}(\xi;\zeta_D + \varsigma)|^2 \,\mathrm{d}\xi, \tag{9}$$

where $\varsigma = s/z_R$ and we considered one dimension only. The signal phase in excess or defect to $-ks$ is given by

$$\phi(\varsigma) = \arg[\Xi(\varsigma)], \tag{10}$$

where

$$\Xi(\varsigma) = \int_{-\infty}^{+\infty} \psi_{\text{rf}}^*(\xi;\zeta_D)\psi_{\text{ms}}(\xi;\zeta_D + \varsigma)\,\mathrm{d}\xi, \tag{11}$$

4

and the star indicates the complex conjugation. Therefore, the period of the travelling fringe is

$$\lambda_e = \lambda\left(1 + \frac{\partial_\varsigma\phi\big|_{\varsigma=0}}{kz_R}\right) = \lambda\left(1 + \frac{\theta_0^2\,\partial_\varsigma\phi\big|_{\varsigma=0}}{2}\right), \quad (12)$$

where $\theta_0^2 = 2/(kz_R)$ is the squared divergence of u_0 and the positive sign is dictated by the $-\mathrm{i}kz$ choice for the cumulated phase, $k = 2\pi/\lambda$ relationship, and the conjugation choice in (11).

For the sake of simplicity, we limited the λ_e calculation to the $\varsigma = 0$ case. This simplification does not mean that we are limiting ourselves to a null difference of the optical paths. However, to ensure that the contamination of the otherwise identical TEM_0 modes is small, the optical-path difference must be smaller than the Rayleigh distance. To go beyond this approximation, we must set the waists of the TEM_0 modes at different distances from the detector or, which is the same, extend the λ_e calculation to the $\varsigma \neq 0$ case.

The extension of (12) to two dimensions is

$$\lambda_e = \lambda\left(1 + \frac{\theta_{01}^2\,\partial_\varsigma\phi_1\big|_{\varsigma=0}}{2} + \frac{\theta_{02}^2\,\partial_\varsigma\phi_2\big|_{\varsigma=0}}{2}\right), \quad (13)$$

where $\theta_{01,02}$ are the principal divergences of the TEM_0 mode of the chosen beam decomposition.

The derivative of $\phi(\varsigma)$ is

$$\partial_\varsigma\phi\big|_{\varsigma=0} = \frac{\mathrm{Im}(\Xi_0'\Xi_0^*)}{|\Xi_0|^2}, \quad (14)$$

with $\Xi_0 = \Xi(\zeta_D)$ and $\Xi_0' = \partial_\varsigma\Xi\big|_{\varsigma=0}$. It must be noted that, as shown in [14, 31], Ξ_0 and Ξ_0' are independent of ς_D. Therefore, without loss of generality, we set $\varsigma_D = 0$.

Our results do not depend on how we draw the phase difference (10) out of the interference signal. Therefore, they apply equally well to the homodyne and heterodyne detections.

3.1. Mismatched beams

We can use the newly developed formalism to study the interference of mismatched beams. Hence, let

$$\psi_{\mathrm{rf}}(\xi;\zeta_D) = u_0(\xi;\zeta_D) + \sum_{n\geq 1} a_n u_n(\xi;\zeta_D) \quad (15a)$$

$$\psi_{\mathrm{ms}}(\xi;\zeta_D) = u_0(\xi;\zeta_D) + \sum_{n\geq 1} b_n u_n(\xi;\zeta_D) \quad (15b)$$

be the interfering beams. Therefore,

$$\Xi_0 = 1 + \sum_{n>0} a_n^* b_n. \quad (16a)$$

Furthermore,

$$\Xi_0' = \int_{-\infty}^{+\infty} \psi_{\mathrm{rf}}^*(\xi;0)\left[\partial_\varsigma\psi_{\mathrm{ms}}(\xi,\varsigma)\right]_{\varsigma=0}\mathrm{d}\xi$$

$$= \gamma_{00} + \sum_{n,m>0} a_n^* b_m \gamma_{nm}, \quad (16b)$$

where

$$\gamma_{nm} = \int_{-\infty}^{+\infty} u_n(\xi;0)\left[\partial_\varsigma u_m(\xi,\varsigma)\right]_{\varsigma=0}\mathrm{d}\xi = \frac{\mathrm{i}c_n c_m}{4}$$

$$\int_{-\infty}^{+\infty}\mathrm{e}^{-2\xi^2}\mathrm{H}_n(\sqrt{2}\xi)\left[4m+1-\frac{1}{2}\mathrm{H}_2(\sqrt{2}\xi)\right]\mathrm{H}_m(\sqrt{2}\xi)\,\mathrm{d}\xi$$

$$= \frac{\mathrm{i}}{4}\begin{cases} 2n+1 & \text{if } m=n \\ -\sqrt{n(n-1)} & \text{if } m=n-2 \\ -\sqrt{(n+2)(n+1)} & \text{if } m=n+2 \\ 0 & \text{otherwise} \end{cases}. \quad (17)$$

In (17), we used [39]

$$\partial_\varsigma u_m\big|_{\varsigma=0} = \frac{\mathrm{i}}{4}\left[4m+1-\frac{1}{2}\mathrm{H}_2(\sqrt{2}\xi)\right]$$
$$\times c_m\mathrm{H}_m(\sqrt{2}\xi)\mathrm{e}^{-\xi^2}, \quad (18a)$$

$$\int_{-\infty}^{+\infty}\mathrm{H}_n(\sqrt{2}\xi)\mathrm{H}_m(\sqrt{2}\xi)\mathrm{e}^{-2\xi^2}\,\mathrm{d}\xi = \frac{\delta_{nm}}{c_n c_m}, \quad (18b)$$

$$\int_{-\infty}^{+\infty}\mathrm{H}_2(\sqrt{2}\xi)\mathrm{H}_n(\sqrt{2}\xi)\mathrm{H}_m(\sqrt{2}\xi)\mathrm{e}^{-2\xi^2}\,\mathrm{d}\xi =$$

$$\frac{1}{c_n c_m}\begin{cases} 4n & \text{if } m=n \\ 2\sqrt{n(n-1)} & \text{if } m=n-2 \\ 2\sqrt{(n+2)(n+1)} & \text{if } m=n+2 \\ 0 & \text{otherwise} \end{cases}. \quad (18c)$$

Eventually, (16b) can be rewritten as

$$\Xi_0' = \frac{\mathrm{i}}{4}\left[1 + \sum_{n>0}(2n+1)a_n^* b_n\right.$$
$$\left. - \sum_{n>1}\sqrt{n(n-1)}(a_n^* b_{n-2} + a_{n-2}^* b_n)\right]. \quad (19)$$

Eventually, when considering a small contamination by parasitic modes of otherwise matched Gaussian beams, by using (19), (16a) and (14) in (12) and considering only the lowest order terms, we obtain

$$\frac{\Delta\lambda}{\lambda} = \frac{\theta_0^2}{8}\left[1 + 2\sum_{n>0}n\,\mathrm{Re}(a_n^* b_n)\right.$$
$$\left. - \sum_{n>1}\sqrt{n(n-1)}\mathrm{Re}(a_n^* b_{n-2} + a_{n-2}^* b_n)\right] \quad (20)$$

where $\Delta\lambda = \lambda_e - \lambda$ and $\theta_0^2 = 2/(kz_R)$ is the squared divergence of the TEM_0 mode.

3.2. Matched beams

The correction for the interference of matched (paraxial) beams is [31],

$$\frac{\Delta\lambda}{\lambda} = \frac{\theta^2}{8}, \quad (21)$$

where θ is the beams' divergence, we take $\psi_{\mathrm{rf}}(\xi;\zeta_D) = \psi_{\mathrm{ms}}(\xi;\zeta_D) = \psi(\xi;\zeta_D)$.

By setting $a_n = b_n$ in (20), we obtain

$$\frac{\Delta\lambda}{\lambda} = \frac{\theta_0^2}{8}\left[1 + 2\sum_{n>0} n\,|a_n|^2 \right.$$

$$\left. - 2\sum_{n>1}\sqrt{n(n-1)}\,\mathrm{Re}(a_n^* a_{n-2})\right], \qquad (22)$$

which, therefore, expresses θ in terms of θ_0 and the ψ's modal expansion.

To reobtain (21) via the new formalism, we can differentiate Ξ under the integral sign. Hence,

$$\Xi_0' = \int_{-\infty}^{+\infty}\psi^*(\xi;0)\big[\partial_\varsigma\psi(\xi,\varsigma)\big]_{\varsigma=0}\mathrm{d}\xi. \qquad (23a)$$

Next, from the paraxial approximation of the wave equation, we derive the identity $\partial_\varsigma = -\mathrm{i}\partial_\xi^2/4$, where $-\partial_\xi^2/w^2$ is the direct space representation of the square of the linear- momentum operator, p^2, and w is the $1/e^2$ radius of the ψ's waist. Hence,

$$\Xi_0' = -\frac{\mathrm{i}}{4}\int_{-\infty}^{+\infty}\psi^*(\xi;0)\partial_\xi^2\psi(\xi,0)\,\mathrm{d}\xi = \frac{\mathrm{i}\sigma_p^2 w^2}{4}, \qquad (23b)$$

where σ_p^2 is the variance of the ψ's momentum-space representation. Without loss of generality, we can assume the optical field normalised. Hence,

$$\Xi_0 = \int_{-\infty}^{+\infty}\psi^*(\xi;0)\psi(\xi,0)\,\mathrm{d}\xi = 1 \qquad (24)$$

and, by using (24) and (23b) in (14),

$$\partial_\varsigma\phi\big|_{\varsigma=0} = \mathrm{Im}(\Xi_0') = \frac{\sigma_p^2 w^2}{4}. \qquad (25)$$

Eventually, since $\theta = 2\sigma_p/k$ is the ψ's divergence,

$$\frac{\Delta\lambda}{\lambda} = \frac{\sigma_p^2}{2k^2} = \frac{\theta^2}{8} \qquad (26)$$

reproduces (21).

4. Gaussian beam interference

Now, we set the z axis collinear to the measure beam axis, whose divergence and waist location fix w_0 and the Hermite-Gauss basis. Therefore, $\psi_{\mathrm{ms}} = u_0$ and the coefficients the ψ_{ms}'s modal expansion are $b_n = \delta_{0n}$.

4.1. Matched beams.

If the measure and reference beams are coaxial and share the waist size and location, that is, if $\psi_{\mathrm{rf}} = \psi_{\mathrm{ms}} = u_0$, their modal expansion are $a_n = b_n = \delta_{0n}$. Hence, (20) predicts correctly that the fractional correction of the interference period of two identical (one-dimensional) Gaussian beams is

$$\frac{\Delta\lambda}{\lambda} = \frac{\theta_0^2}{8}, \qquad (27)$$

where $\theta_0 = \sqrt{2/(kz_R)}$ is the divergence of both the reference and measure beams.

According to (6b), if we use a basis having the waist displaced by ζ_0, the lowest-order coefficients of the beams' expansion are

$$\boldsymbol{a} = \boldsymbol{b} = \left\{1, 0, -\frac{\zeta_0(2\mathrm{i}-\zeta_0)}{4\sqrt{2}}, 0, -\sqrt{\frac{3}{2}}\frac{\zeta_0^2}{8}\right\}. \qquad (28)$$

In this case, $\Xi_0 = 1 - \zeta_0^2/8$ and $\Xi_0' = (\mathrm{i} + \zeta_0 - \mathrm{i}\zeta_0^2/8)/4$. By calculating $\partial_\varsigma\phi\big|_{\zeta_0}$ according to (14), $\Delta\lambda/\lambda = \theta_0^2/8$ follows again. This confirms that the beam representation does not affect the λ_e calculation.

4.2. Beam axis mismatch.

If the interfering beams are not coaxial, from (5b), their modal expansions are $\boldsymbol{a} = \{1, \xi_0, \xi_0^2/\sqrt{2}\}$ and $b_n = \delta_{0n}$, where ξ_0 is a small axis offset. Therefore, $\Xi_0 = 1$ and $\Xi_0' = \mathrm{i}(1 - \xi_0^2)/4$. Eventually, from (14) and (12),

$$\frac{\Delta\lambda}{\lambda} = \frac{\theta_0^2}{8}(1 - \xi_0^2), \qquad (29)$$

which confirms the result obtained in [14] via Fourier optics.

4.3. Wavefront tilt.

From (4b), the modal expansion of tilted beams are $\boldsymbol{a} = \{1, -\mathrm{i}\tilde{\alpha}/2, -\tilde{\alpha}^2/(4\sqrt{2})\}$ and $b_n = \delta_{0n}$, where $\tilde{\alpha} = kw_0\alpha$ and α is a small tilt angle. Therefore, $\Xi_0 = 1$ and $\Xi_0' = \mathrm{i}(1 - \tilde{\alpha}^2/4)/4$. Eventually,

$$\frac{\Delta\lambda}{\lambda} = \frac{\theta_0^2 + \alpha^2}{8}, \qquad (30)$$

which agrees with the result given in [14]. It is worth noting that $\theta_0^2 + \alpha^2$ is the second moment of the angular spectrum of ψ_{rf} calculated with respect to the direction of the ψ_{ms} axis.

4.4. Waist location mismatch.

If the beam path-lengths through the interferometer differ by ζ_0, their waists are spaced by ζ_0, where $\zeta_0^2 \ll 1$ ensures the validity of the approximations made. Hence, from (6b), the modal expansion of the interfering beams are

$$\boldsymbol{a} = \left\{1, 0, -\frac{\zeta_0(2\mathrm{i}-\zeta_0)}{4\sqrt{2}}, 0, -\sqrt{\frac{3}{2}}\frac{\zeta_0^2}{8}\right\} \qquad (31)$$

and $b_n = \delta_{0n}$. Therefore, $\Xi_0 = 1$ and $\Xi_0' = (\mathrm{i} + \zeta_0 + \mathrm{i}\zeta_0^2/8)/4$. Eventually,

$$\frac{\Delta\lambda}{\lambda} = \frac{\theta_0^2}{8}\left(1 - \frac{\zeta_0^2}{4}\right). \qquad (32)$$

which was never derived before.

6

4.5. Waist radius mismatch.

When the interfering beams have not the same waist radius, from (7b), their modal expansions are $\boldsymbol{a} = \{1, 0, \upsilon/\sqrt{2}\}$ and $b_n = \delta_{0n}$, where $(1+\upsilon)w_0$ and w_0 are the waist radii. Therefore, $\Xi_0 = 1$ and $\Xi'_0 = \mathrm{i}(1-\upsilon)/4$. Eventually,

$$\frac{\Delta\lambda}{\lambda} = \frac{\theta_0^2}{8}(1 - \upsilon), \tag{33}$$

which was never derived before.

In (20), apart from the $\upsilon = \sqrt{2}\mathrm{Re}(a_2 + b_2)$ term, all the fractional corrections to $\theta_0^2/8$ are of the second order. Therefore, the mismatch of the waist radii causes the most significant deviation from $\theta_0^2/8$. Also, identical mismatches, that is, $\mathrm{Re}(a_2) = \mathrm{Re}(b_2)$, only means that the choice of the TEM_0 mode was not optimal.

To investigate further into the matter, let $\overline{\theta^2} = (\theta_{\mathrm{rf}}^2 + \theta_{\mathrm{ms}}^2)/2$ be the mean of the squared divergences of the reference and measure beams, $\theta_{\mathrm{rf}} = \theta_0/(1+\upsilon)$ and $\theta_{\mathrm{ms}} = \theta_0$, respectively. Hence, (33) can be rewritten as

$$\frac{\Delta\lambda}{\lambda} = \frac{\overline{\theta^2}}{8}. \tag{34}$$

Furthermore, if the mismatches are identical, that is, if $\boldsymbol{a} = \boldsymbol{b} = \{1, 0, \upsilon/\sqrt{2}\}$, then, as expected,

$$\frac{\Delta\lambda}{\lambda} = \frac{\theta_0^2}{8}(1 - 2\upsilon) = \frac{\theta^2}{8}, \tag{35}$$

where $\theta \approx \theta_0(1-\upsilon)$ is the divergence of the interfering beams.

4.6. Wavefront mismatch.

If the interfering beams share neither the waist location nor the radius, from (8b), their modal expansions are

$$\boldsymbol{a} = \left\{1, 0, -\frac{\kappa(2\mathrm{i} + \kappa)}{4\sqrt{2}}, 0, -\sqrt{\frac{3}{2}}\frac{\kappa^2}{8}\right\} \tag{36}$$

and $b_n = \delta_{0n}$, where κ is the curvature of the $\zeta = \zeta_D$ reference wavefront. Therefore, $\Xi_0 = 1$ and $\Xi'_0 = (\mathrm{i} - \kappa/2 - \mathrm{i}\kappa^2/4)/4$. Eventually,

$$\frac{\Delta\lambda}{\lambda} = \frac{\theta_0^2}{8}\left(1 + \frac{\kappa^2}{4}\right). \tag{37}$$

After noting that the waist of the reference beam, having $1 - \kappa^2/2$ radius, is located in $\zeta_{\mathrm{rf}} = -\kappa$, by using (32), the correction is

$$\frac{\Delta\lambda}{\lambda} = \frac{\overline{\theta^2}}{8}\left(1 - \frac{\zeta_{\mathrm{rf}}^2}{4}\right), \tag{38}$$

which, by using $\theta_{\mathrm{rf}} = \theta_0/(1 - \kappa^2/2)$ and $\theta_{\mathrm{ms}} = \theta_0$, can also be proven identical to (34).

4.7. Hermite-Gauss beams

In the case of matched Hermite-Gauss beams, that is, when $\psi_{\mathrm{rf}} = \psi_{\mathrm{ms}} = u_n$, the modal expansion of the interfering beams are $a_l = b_l = \delta_{ln}$. Therefore, $\Xi_0 = 1$ and $\Xi'_0 = (2n + 1)\mathrm{i}/4$. Eventually,

$$\frac{\Delta\lambda}{\lambda} = \frac{\theta_l^2}{8}, \tag{39}$$

where $\sqrt{2n+1}\,\theta_0$ is the u_n divergence.

5. Statistical considerations

Estimating of the correction of the fringe period (20) requires the knowledge of the complex amplitudes of both the interfering beams. In the absence of such a detailed information, we can rely on statistical considerations. To this end, we fix the norm of the beam residuals from the TEM_0 mode. Hence,

$$\int_{-\infty}^{+\infty} \left|\psi_{\mathrm{rf}}(\xi; \zeta) - u_0(\xi; \zeta)\right|^2 \mathrm{d}\xi = \sum_{n=1}^{N} |a_n|^2 = \rho^2 \quad (40a)$$

and

$$\int_{-\infty}^{+\infty} \left|\psi_{\mathrm{ms}}(\xi; \zeta) - u_0(\xi; \zeta)\right|^2 \mathrm{d}\xi = \sum_{n=1}^{N} |b_n|^2 = \rho^2, \quad (40b)$$

where we assumed the same bandwidth, N, and residual norm, ρ. Also, by taking advantage of the non-uniqueness of the Hermite-Gauss decomposition, we minimise ρ^2 by choosing the TEM_0 mode simultaneously best fitting both ψ_{rf} and ψ_{ms}.

In the absence of additional information, the joint probability distribution of the a_n and b_n coefficients is uniform over two $2N$-spheres about the origin of ρ radius. Consequently, the average correction is

$$\left\langle \frac{\Delta\lambda}{\lambda} \right\rangle = \frac{\theta_0^2}{8} \left[\frac{2\pi^N}{\Gamma(N)}\right]^{-2}$$

$$\times \int_{S_a} \int_{S_b} \left[1 + 2\rho^2 \sum_{n>0}^{N} n\,\mathrm{Re}(\alpha_n^*\beta_n) - \rho\sqrt{2}\mathrm{Re}(\alpha_2^* + \beta_2)\right.$$

$$\left. -\rho^2 \sum_{n>2}^{N} \sqrt{n(n-1)}\mathrm{Re}(\alpha_n^*\beta_{n-2} + \alpha_{n-2}^*\beta_n)\right] \mathrm{d}\varsigma_a \mathrm{d}\varsigma_b$$

$$= \frac{\theta_0^2}{8}, \tag{41}$$

where $\alpha_n = a_n/\rho$, $\beta_n = b_n/\rho$, S_a and S_b are $2N$-spheres about the origin of unit radius, $2\pi^N/\Gamma(N)$ is the $(2N-1)$-dimensional area of $S_{a,b}$, and $\mathrm{d}\varsigma_{a,b}$ are the relevant elements of area. Reference [40] explains how integrating a polynomial over a hypersphere. Equation (41) shows that $\theta_0^2/8$ is an unbiased estimate and confirms and extends the validity of the numerical results given in [35].
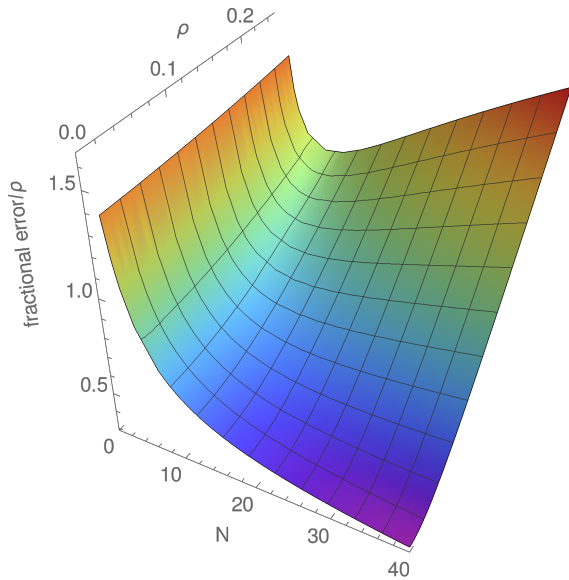
Figure 1. Fractional standard deviation $\sigma_{\lambda_e}/\lambda$ of the effective wavelength normalised to the residual norm ρ.

The fractional variance of λ_e is

$$\left(\frac{\sigma_{\lambda_e}}{\lambda}\right)^2 = \left[\frac{2\pi^N}{\Gamma(N)}\right]^{-2}$$

$$\times \int_{S_a}\int_{S_b}\left[2\rho^2\sum_{n>0}^{N} n\,\mathrm{Re}(\alpha_n^*\beta_n) - \rho\sqrt{2}\mathrm{Re}(\alpha_2^* + \beta_2)\right.$$

$$\left. -\rho^2\sum_{n>2}^{N}\sqrt{n(n-1)}\mathrm{Re}(\alpha_n^*\beta_{n-2} + \alpha_{n-2}^*\beta_n)\right]^2 \mathrm{d}\varsigma_a\mathrm{d}\varsigma_b$$

$$= \begin{cases} 2\rho^4 & \text{if } N = 1 \\ \dfrac{4\rho^2}{N} + \dfrac{(N^3 + N^2 - 2)\rho^4}{N^2} & \text{if } N \geq 2 \end{cases}.$$

$$(42)$$

The $4\rho^2/N$ term comes from the first order correction to $\theta_0/8$ due to the mismatch of the waist radii – the $\sqrt{n(n-1)}\mathrm{Re}(a_n^*b_{n-2} + a_{n-2}^*b_n)$, where $n = 2$, term in (20). All the other aberrations and mismatches originate second-order corrections. Consequently, their contributions to the fractional variance are proportional to ρ^4. Figure 1 shows how the fractional standard deviation of the effective wavelength depends on the residual norm and bandwidth.

From these results, we guess that calculations based on the divergences of the interfering beams overestimate $\Delta\lambda/\lambda$, as empirically observed in [35]. To confirm this heuristic we can average (22) over the S_a hypersphere. Hence,

$$\langle\theta^2\rangle = \theta_0^2\frac{\Gamma(N)}{2\pi^N}$$

$$= \times \int_{S_a}\left[1 + 2\rho^2\sum_{n>0} n\,|\alpha_n|^2 - 2\sqrt{2}\rho\mathrm{Re}(\alpha_2)\right.$$

$$\left. -2\rho^2\sum_{n>1}\sqrt{n(n-1)}\,\mathrm{Re}(\alpha_n^*\alpha_{n-2})\right]\mathrm{d}\varsigma_a$$

$$= \theta_0^2\left[1 + (1 + N)\rho^2\right]. \tag{43}$$

confirms the overestimation.

By using the $\sigma_{\lambda_e}/\lambda = 0.12$ and $(\langle\theta^2\rangle - \theta_0^2)/\theta_0^2 = 0.63$ values obtained in [35] in (42) and (43), and excluding a mismatches of the waist radii (not considered in [35]), the estimates $\rho \approx 0.15$ and $N \approx 27$ follow. Although the numerical simulation in [35] did not fix these parameters, these values are in reasonable agreement with what is expected.

6. Conclusions

Unless they are plane waves, optical fields do not have well defined wavelengths. In fact, because of diffraction, the distance travelled by wavefronts during one oscillation period differs from the plane wave one and varies from one point to another. Therefore, the relationship between the accumulated phase and the distance travelled requires corrections that depend on the measurement procedure and modal spectra of the interfering beams.

When two matched Gaussian beams interfere and the arm difference is much smaller than the Rayleigh distance, the period of the integrated interference differs from the plane-wave wavelength by a quarter of the beams' squared-divergence (in relative terms) [31]. We reported an analytical study of additional errors related to mismatches and contaminations by parasitic modes [34].

Firstly, we re-obtained and strengthen known results by using a new mathematical approach based on the modal expansion of the optical field. Secondly, the newly developed formalism was used to study analytically the effect of mismatches and aberrations that we previously tackled only numerically [35].

To calculate the sought correction, it is necessary to know the wavefront profiles of the interfering beams, which are difficult to measure with the needed resolution and accuracy. Therefore, we resorted to statistical considerations and proved that an estimate based on the divergence of the TEM_0 mode simultaneously fitting both the interfering beams is unbiased. This result was previously only inferred from numerical simulations [35].

Also, we evaluated the uncertainty of this estimate, in terms of the fit-residuals norm. Eventually, we confirmed that the divergence of the interfering beams is a biased estimator and that, on the average, it overestimates the correction.

Our results indicate that the beams used in high accuracy length measurements by interferometry need to be also characterised as regards as the modal spectra. Statements quantifying or excluding contaminations by parasitic modes should be added to those dealing with the frequency.

Appendix

In the subsections from 2.1.1 to 2.1.5, we decomposed the complex amplitudes of paraxial beams into superpositions of Hermite-Gauss modes. Next, the modal amplitudes were expanded up to the second order of the small mismatches. This appendix gives some details of the calculations [41].

Wavefront tilt (section 2.1.1). By substituting $(4a)$ for $\psi(\xi;0)$ in (3), we get the integrals

$$A_0 = \int_{-\infty}^{+\infty} e^{-\xi^2 - i\tilde{\alpha}\xi} u_0(\xi;0)\, d\xi, \tag{A.1}$$

$$a_n = \frac{1}{A_0} \int_{-\infty}^{+\infty} e^{-\xi^2 - i\tilde{\alpha}\xi} u_n(\xi;0)\, d\xi. \tag{A.2}$$

Eventually $a_0 = 1$ and,

$$A_0 = \sqrt[4]{\pi/2}\, e^{-\tilde{\alpha}^2/8}, \tag{A.3}$$

$$a_1 = -i\tilde{\alpha}/2, \tag{A.4}$$

$$a_2 = -\tilde{\alpha}^2/(4\sqrt{2}). \tag{A.5}$$

The modes higher than TEM_2 are omitted because their amplitudes involve only powers of $\tilde{\alpha}$ higher than two.

Beam axis mismatch (section 2.1.2). By substituting $(5a)$ for $\psi(\xi;0)$ in (3), we get integrals similar to (A.1-2). Hence $a_0 = 1$ and,

$$A_0 = \sqrt[4]{\pi/2}\, e^{-\xi_0^2/2}, \tag{A.6}$$

$$a_1 = \xi_0, \tag{A.7}$$

$$a_2 = \xi_0^2/\sqrt{2}. \tag{A.8}$$

The modes higher than TEM_2 are omitted because their amplitudes involve only powers of ξ_0 higher than two.

Waist location mismatch (section 2.1.3). By using $(6a)$ in (3), we get $a_0 = 1$ and

$$A_0 = \sqrt[4]{2\pi}\sqrt{\frac{i + \zeta_0}{2i + \zeta_0}}, \tag{A.9}$$

$$a_2 = \frac{\zeta_0}{\sqrt{2}(2i + \zeta_0)}, \tag{A.10}$$

$$a_4 = \sqrt{3/2}\, a_2^2. \tag{A.11}$$

The odd-mode amplitudes are null. The modes higher than TEM_4 are omitted because their amplitudes involve ζ_0 power higher than two.

Waist radius mismatch (section 2.1.4). By using $(7a)$ in (3), we get $a_0 = 1$ and

$$A_0 = \frac{\sqrt[4]{2\pi}(1+\upsilon)}{\sqrt{2 + \upsilon(2 + \upsilon)}}, \tag{A.12}$$

$$a_2 = \frac{\upsilon(2 + \upsilon)}{\sqrt{2}\left[2 + \upsilon(2 + \upsilon)\right]}, \tag{A.13}$$

$$a_4 = \sqrt{3/2}\, a_2^2. \tag{A.14}$$

The odd-mode amplitudes are null. The modes higher than TEM_4 are omitted because their amplitudes involve *upsilon* power higher than two.

Wavefront curvature mismatch.(section 2.1.5). By using $(8a)$ in (3), we get $a_0 = 1$ and

$$A_0 = \frac{\sqrt[4]{2\pi}}{\sqrt{2 + i\kappa}}, \tag{A.15}$$

$$a_2 = \frac{\kappa}{\sqrt{2}(2i - \kappa)}, \tag{A.16}$$

$$a_4 = \sqrt{3/2}\, a_2^2. \tag{A.17}$$

The odd-mode amplitudes are null. The modes higher than TEM_4 are omitted because their amplitudes involve κ power higher than two.

References

[1] Bureau International des Poids et Mesures 2006 The International System of Units (SI) 8th edition updated in 2014 www.bipm.org/en/publications/si-brochure/metre.html Accessed: 2018-12-20

[2] Cavagnero G, Fujimoto H, Mana G, Massa E, Nakayama K and Zosi G 2004 *Metrologia* **41** 445–446

[3] Galzerano G, Mana G and Massa E 2007 *Measurement Science and Technology* **18** 1338–1342

[4] Stone J A, Decker J E, Gill P, Juncar P, Lewis A, Rovera G D and Viliesid M 2009 *Metrologia* **46** 11–18

[5] Schoedel R and Franke P 2019 *Metrologia* **56** 015009

[6] Berry M 1987 *Journal of Modern Optics* **34** 1401–1407

[7] Bergamin A, Cavagnero G and Mana G 1992 *Journal of Modern Optics* **39** 2053–2074

[8] Massa E, Mana G, Krempel J and Jentschel M 2013 *Opt. Express* **21** 27119–27126

[9] Dorenwendt K and Boensch G 1976 *Metrologia* **12** 57–60

[10] Mana G 1989 *Metrologia* **26** 87–94

[11] Bergamin A, Cavagnero G and Mana G 1994 *Phys. Rev. A* **49**(3) 2167–2173

[12] Bergamin A, Cavagnero G, Cordiali L and Mana G 1997 *IEEE Transactions on Instrumentation and Measurement* **46** 196–200

[13] van Westrum D and Niebauer T M 2003 *Metrologia* **40** 258–263

[14] Cavagnero G, Mana G and Massa E 2006 *J. Opt. Soc. Am. A* **23** 1951–1959

[15] Robertsson L 2007 *Metrologia* **44** 35–39

[16] Fujimoto H, Mana G and Nakayama K 2007 *IEEE Transactions on Instrumentation and Measurement* **56** 351–355

[17] D'Agostino G and Robertsson L 2011 *Applied Physics B* **103** 357–361

[18] Andreas B, Ferroglio L, Fujii K, Kuramoto N and Mana G 2011 *Metrologia* **48** S104–S111

[19] Andreas B, Fujii K, Kuramoto N and Mana G 2012 *Metrologia* **49** 479–486

[20] Andreas B, Mana G and Palmisano C 2015 *J. Opt. Soc. Am. A* **32** 1403–1424

[21] Andreas B, Mana G and Palmisano C 2016 *J. Opt. Soc. Am. A* **33** 559–560

[22] Mana G, Massa E and Sasso C P 2018 *Metrologia* **55** 222–229

[23] Robinson I A and Schlamminger S 2016 *Metrologia* **53** A46–A74

[24] Rainville S, Thompson J, Myers E, Brown J, Dewey M, Kessler Jr E, Deslattes R, Börner H, Jentschel M, Mutti P and Pritchard D 2005 *Nature* **438** 1096–1097

[25] Fujii K, Massa E, Bettin H, Kuramoto N and Mana G 2018 *Metrologia* **55** L1–L4

[26] Mai T and Nicolaus A 2017 *Metrologia* **54** 487–493

[27] Sasso C P, Mana G and Mottini S 2018 *Classical and Quantum Gravity* **35** 185013

[28] Sasso C P, Mana G and Mottini S 2018 *Classical and Quantum Gravity* **35** 245002

[29] Sasso C P, Mana G and Mottini S 2019 *Optics Express* **27** 16855

[30] Wanner G and Heinzel G 2014 *Appl. Opt.* **53** 3043–3048

[31] Bergamin, A, Cavagnero, G, Cordiali, L and Mana, G 1999 *Eur. Phys. J. D* **5** 433–440

[32] Mana G, Massa E, Sasso C P, Andreas B and Kuetgens U 2017 *Metrologia* **54** 559–565

[33] Balsamo A, Cavagnero G, Mana G and Massa E 2003 *Journal of Optics A: Pure and Applied Optics* **5** 418–424

[34] Sasso C P, Massa E and Mana G 2016 *Opt. Express* **24** 6522–6531

[35] Mana G, Massa E and Sasso C P 2018 *Metrologia* **55** 535–540

[36] Morrison E, Meers B J, Robertson D I and Ward H 1994 *Appl. Opt.* **33** 5041–5049

[37] Levy U, Derevyanko S and Silberberg Y 2016 Light modes of free space *Progress in Optics* vol 61 ed Visser T D (Elsevier) pp 237–281

[38] Siegman A E 1986 *Lasers* (University Science Books)

[39] Marichev O and Trott M 2018 Mathematical functions site `http://functions.wolfram.com/05.01.21.0018.01`, `http://functions.wolfram.com/05.01.21.0019.01`, `http://functions.wolfram.com/05.01.21.0020.01` Accessed: 2018-12-20

[40] Folland G B 2001 *The American Mathematical Monthly* **108** 446–448

[41] Wolfram Research, Inc 2017 Mathematica, Version 11.1 Champaign, IL